Long-Wave Infrared Frequency Comb Generator for Chemical Agent and Explosive Precursor Detection

Ergun Simsek, Pradyoth Shandilya, Raonaqul Islam, Sanzida Akter, and Curtis R. Menyuk

University of Maryland Baltimore County, 1000 Hilltop Circle, 21250 Baltimore, MD, USA

ABSTRACT

We present the design and numerical characterization of a CMOS-compatible silicon-in-zinc selenide (Si–ZnSe) micro-ring resonator for soliton frequency comb generation in the long-wave infrared (LWIR) band. The proposed device is engineered to operate within the 9.5–12 μm range, corresponding to the molecular fingerprint region of chemical warfare agents, explosive precursors, and emerging opioid analogs. By leveraging the high nonlinear refractive index of silicon and the low optical absorption of ZnSe, the structure achieves strong field confinement and efficient Kerr nonlinear interactions while mitigating mid-IR loss mechanisms. Using a mixed-field finite-difference solver, we extract the effective indices and compute the integrated dispersion, demonstrating an exceptionally flat profile below 150 MHz integrated dispersion across the entire spectral window. The micro-ring exhibits a free spectral range of approximately 60 GHz, matching the detection bandwidth of high-speed photodiodes. We further solve the normalized Lugiato–Lefever equation using a symmetric split-step Fourier method to model soliton dynamics within the resonator. Simulation results confirm the generation of stable dissipative Kerr solitons with a broadband comb spectrum exhibiting slow spectral roll-off, indicating strong nonlinear coupling and low phase mismatch. The resulting frequency comb spans multiple micrometers in the LWIR, enabling simultaneous multi-species detection. This integrated platform offers compactness, scalability, and compatibility with existing semiconductor manufacturing processes. The combination of wide spectral coverage, high sensitivity, and CMOS compatibility positions this technology as a promising foundation for portable, field-deployable spectroscopic systems capable of real-time identification of hazardous chemicals, explosive precursors, and fentanyl-like opioids in complex environments.

Keywords: Frequency combs, solitons, spectroscopy, long-wave infrared, silicon photonics

1. INTRODUCTION

Detection of chemical warfare agents and explosive precursors (CWAEPs) in realistic environments requires sensing systems that are highly sensitive, selective, and capable of broadband operation. The long-wave infrared (LWIR) spectral region, particularly between 7.8 and 13.8 μm as shown in Fig. 1(a), coincides with the unique and strong vibrational absorption fingerprints of many CWAEPs such as sarin, soman, cyclosarin, and tabun as shown in Fig. 1(b), as well as fentanyl-like opioids as shown in Fig. 1(c). This molecular fingerprint region is also advantageous because it avoids interference from atmospheric constituents, providing an excellent opportunity for standoff detection using frequency comb spectroscopy.[1–3] Including the opioid spectrum further demonstrates the versatility of the sensing platform for detecting not only chemical warfare agents but also emerging public health threats such as synthetic opioids and their adulterants.

A photonic frequency comb converts a single-frequency laser into a set of evenly spaced spectral lines spanning a broad wavelength range.[1–7] Each comb line serves as a precise frequency reference, enabling high-resolution molecular spectroscopy. By analyzing attenuation at specific comb lines, the presence and, if present, concentration of CWAEPs can be determined.

In this work, we present a novel, integrated silicon-in-ZnSe micro-ring resonator platform designed for highly-stable LWIR soliton frequency comb generation, as shown in Fig. 2. In this setup, an infrared pump laser near 10.6 μm is coupled into a bus waveguide adjacent to the ring resonator. Nonlinear processes within the microresonator broaden the pump into a dense frequency comb. The comb is then used for spectroscopy through a gas cell or open-air path. Spectral attenuation of the precisely-spaced comb lines provides a high-resolution signature that enables simultaneous identification and concentration monitoring of multiple CWAEPs.

Further author information: (Send correspondence to E. S.) E-mail: simsek@umbc.edu, Telephone: 1 410 455 3540

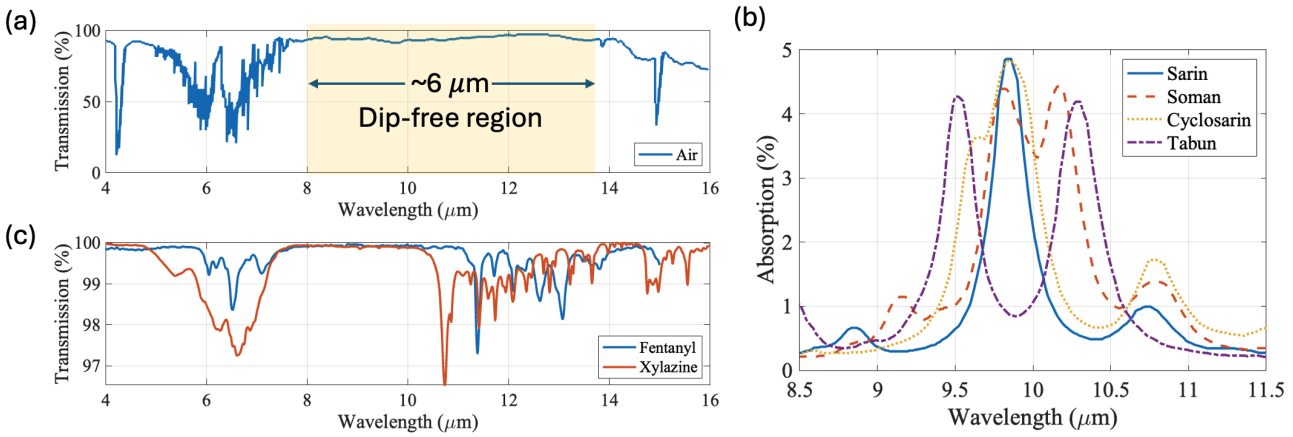

Figure 1: (a) Transmission spectrum of air has a clear window for the wavelengths from 7.8 μm to 13.8 μm. (b) Absorption spectra of various chemical warfare agents in the LWIR region. (c) Transmission spectrum of fentanyl and Xylazine

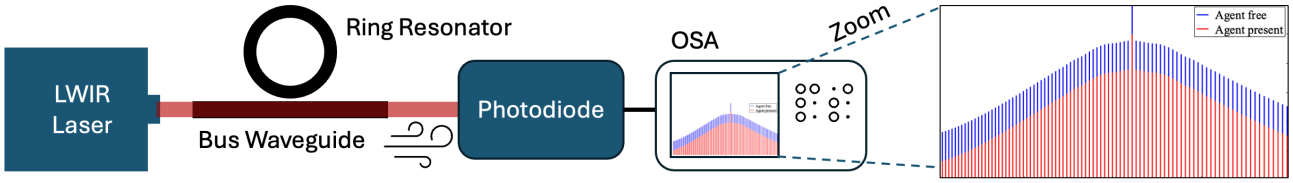

Figure 2: Schematic of the proposed LWIR frequency comb spectroscopy system. The microresonator-based comb generator enables real-time identification of hazardous agents through spectral absorption analysis.

2. DEVICE DESIGN WITH NUMERICAL SOLVERS

The proposed micro-ring resonator features a silicon core embedded in a ZnSe cladding, forming a silicon-in-ZnSe configuration. The silicon core has a thickness of 3 μm, a width of 11 μm, and an outer radius of 230 μm. The large refractive index contrast between Si[8] and ZnSe[9] provides strong optical confinement within the silicon core, resulting in high intra-cavity optical intensities. This strong field localization enhances the effective nonlinear interaction length and thereby facilitates efficient Kerr nonlinear processes such as spectral broadening. Meanwhile, the ZnSe cladding serves to suppress the otherwise significant optical absorption losses of silicon in the long-wave infrared (LWIR) region. To take ZnSe's dispersion into account accurately in the LWIR region, we adopt the Sellmeier-type relation, Eq. (1), with the coefficients given in Table 1.

$$\varepsilon_r^{\mathrm{ZnSe}}(\lambda) = 1 + \sum_{i=1}^{3} \frac{A_i \lambda^2}{\lambda^2 - B_i} \qquad (1)$$

Table 1: Dispersion model parameters for ZnSe.

i	A_i	B_i
1	2.364510	0.295839
2	2.465825	0.295839
3	0.843897	1000

A tunable CO_2 laser operating near 10.6 μm is considered as the pump source. To match the detection capabilities of available photodiodes with a 67 GHz bandwidth, the resonator design targets a free spectral range (FSR) of approximately 60 GHz.

We calculate the effective refractive index of the ring resonator over the wavelength range of 9.5–12 μm using our recently developed finite-differences–based numerical solver.[6] Figure 3 illustrates the three orthogonal components of the electric field intensity in the ρ–z plane for the first resonant mode for $\lambda = 10.6$ μm, and the ring outer radius, width, and height are 230 μm, 11 μm, and 3 μm, respectively. A strong and asymmetric optical confinement is clearly observed, indicating efficient localization of the electromagnetic field within the silicon core.

From these values, we derive the integrated dispersion as follows. The procedure begins with determining

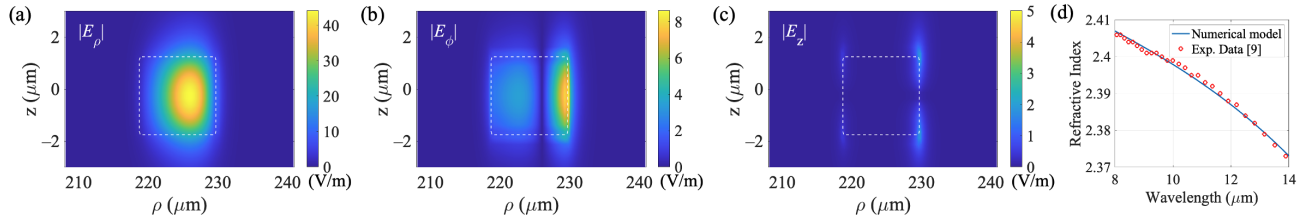

Figure 3: Spatial distribution of the electric field's (a) ρ, (b) ϕ, and (c) z components in the ρ–z plane for the fundamental resonant mode at an excitation wavelength of 10.6 μm. The calculated effective index is $n_{\text{eff}} = 3.21$. The white dashed lines indicate the interface between the Si and ZnSe regions. (d) Refractive index of ZnSe calculated with the parameters in Table 1 vs. the experimental values.[8]

the group index n_g, from which the approximate free spectral range (FSR) can be estimated as $\text{FSR}_{\text{approx}} \approx c_0/2\pi n_g R_c$, where c_0 is the speed of light in vacuum and R_c is the resonator's central radius.

Let f_0 denote the resonant frequency corresponding to the pump wavelength. Near f_0, the propagation constant $\beta(f)$ can be approximated by a first-order Taylor expansion, $\beta(f) \approx \beta_0 + D_1(f - f_0)$, where $\beta_0 = \beta(f_0)$ and $D_1 = \frac{d\beta}{df}\Big| f_0$ represents the first-order frequency spacing. The integrated dispersion is then defined as the deviation from this linear approximation, $D\text{int}(f) = \beta(f) - \beta_0 - D_1(f - f_0)$. The discrete resonances of the ring are characterized by the azimuthal mode number m, which satisfies the resonance condition $m = \beta R_c$. In theory, resonance occurs when m is an integer; however, the values obtained from βR_c are generally non-integer. To address this, we first identify the mode whose resonance frequency is closest to the pump frequency f_0. Around this point, we construct a continuous function $m(f) = \beta(f)R_c$ and generate a corresponding integer mode index array m_i by rounding to the nearest integers within the spectral range of interest. The effective indices $n_{\text{eff}}(\lambda)$ obtained from the mode solver are interpolated onto this integer mode grid, yielding $n_{\text{eff},i}$. The resonance frequencies are then computed as $f_i = c_0 m_i / n_{\text{eff},i} R_c$, and the corresponding wavelengths follow as $\lambda_i = c_0/f_i$. To express the frequency spacing relative to the pump mode, we define the relative mode number $\mu = m_i - m_{i,\text{pump}}$, where $m_{i,\text{pump}}$ corresponds to the integer mode index nearest to the pump resonance. Finally, the integrated dispersion on this integer grid is evaluated as $D_{\text{int}}(\mu) = f_\mu - f_0 - D_1\mu$, where f_μ denotes the resonance frequency calculated via interpolation at integer μ. The resulting $D_{\text{int}}(\mu)$ curve quantifies the deviation from uniform frequency spacing and serves as a key indicator of the resonator's dispersion characteristics. The resulting $D_{\text{int}}/2\pi$ curve, shown in Fig. 4(a), remains exceptionally low (< 150 MHz) over the entire 2.5 μm simulated range. This very low and flat dispersion profile, a key design goal, is crucial for minimizing phase mismatch, allowing for a broadband soliton formation. The device FSR is determined to be approximately 60 GHz.

We solve the normalized Lugiato–Lefever equation (LLE) to model soliton dynamics.[4,5] The normalized LLE can be written as

$$\frac{\partial \psi}{\partial \tau} = -(1 + i\alpha)\psi + i\gamma|\psi|^2\psi - i\frac{\beta_2}{2}\frac{\partial^2 \psi}{\partial \theta^2} + F, \tag{2}$$

where ψ represents the normalized field amplitude, τ is the normalized time, α denotes the detuning between the pump laser and cavity resonance, γ is the nonlinear coefficient, β_2 is the group-velocity dispersion parameter, θ is the azimuthal coordinate along the resonator circumference, and F corresponds to the normalized pump field.

To simulate the time evolution of Eq. (2) efficiently and accurately, the split-step Fourier method is employed.[5] This numerical approach takes advantage of the fact that different terms in the equation are more conveniently handled in different domains. The linear terms, which involve dispersion and loss, are efficiently computed in the Fourier domain, whereas the nonlinear Kerr term is more naturally treated in the time (or angular) domain. In this scheme, each integration step is divided into fractional substeps: the field is first transformed into the Fourier domain to evolve according to the linear operator, then returned to the time domain to evolve under the nonlinear operator. Because the linear and nonlinear operators do not commute, the order in which they are applied introduces a first-order numerical error. To mitigate this, a symmetric (second-order) split-step scheme is used—performing a half-step of the linear evolution, followed by a full-step of the nonlinear evolution, and concluding with another half-step of the linear evolution.

For the LLE simulations, we assumed an optical quality factor (Q) of 10^6. This value was deliberately chosen to account for the expected higher absorption and scattering losses in LWIR operation compared to near-infrared devices. Figure 4(b) shows the simulated soliton amplitude as a function of the angular coordinate θ. The corresponding power spectrum in Fig. 4(c) demonstrates broadband frequency comb formation with a slow spectral roll-off, indicating strong nonlinear coupling among spectral components. From Fig. 4(c), the FSR is determined to be 59.9 GHz. Because the comb spans multiple micrometers across the LWIR band, the same device can detect several species simultaneously. After successful laboratory testing using an optical spectrum analyzer, we plan to integrate a photodiode array to measure the power of individual comb lines electronically, enabling compact, portable, and real-time detection systems.

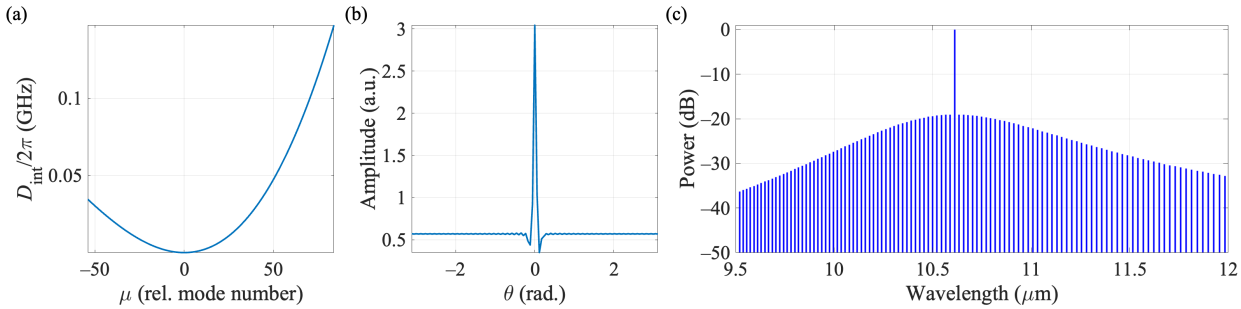

Figure 4: Simulation results for the Si–ZnSe micro-ring resonator. (a) Integrated dispersion $D_{\text{int}}/2\pi$ versus relative mode number μ. (b) Temporal soliton amplitude profile. (c) Soliton frequency comb power spectrum, obtained with setting $F = 2.5$ and $\alpha = 4.6$ in Eq. (2).

3. FUTURE WORK: OPTIMIZATION OF COUPLING AND FABRICATION

To transition from numerical modeling to a physical device, the coupling efficiency between the bus waveguide and the micro-ring resonator must be optimized. In our future work, we will conduct a series of coupled-mode theory (CMT) analyses to determine the optimum gap distance that ensures the resonator operates in the critical coupling or slightly over-coupled regime for maximum power transfer. This analysis requires precise knowledge of the bus waveguide's propagation characteristics; to this end, we will employ a specialized finite-difference frequency-domain solver designed for straight dielectric waveguides[10,11] to extract its effective index. By systematically varying the waveguide geometry and the gap width, we aim to finalize the device parameters. Subsequently, we plan to carry out experimental studies to demonstrate stable dissipative Kerr soliton generation within the LWIR range, validating our integrated Si–ZnSe platform for practical sensing applications.

4. CONCLUSION

We have successfully designed and numerically analyzed a silicon-in-ZnSe micro-ring resonator platform capable of generating stable dissipative Kerr soliton frequency combs in the 9.5-12 μm LWIR band with a 60 GHz FSR. Our unique design achieves an ultra-low and flat integrated dispersion below 150 MHz, which is essential for broadband operation. By combining the CMOS compatibility of silicon with the LWIR transparency of ZnSe, this platform offers a viable path toward compact, high-sensitivity, and field-deployable spectroscopic detection systems for chemical warfare agents and explosive precursors.

Acknowledgments

This work has been supported in part by cooperative agreements with the National Center for Manufacturing Sciences 2022138-142232 and 2023200-142386, which are sub-contracts from the US-DoD cooperative agreements HQ0034-20-2-0007 and HQ0034-24-2-0001, respectively.

Data availability

The code to reproduce the results provided in this manuscript can be found at https://github.com/simsekergun/DieRingSolver.

REFERENCES

[1] Schliesser, A., Brehm, M., Keilmann, F., and van der Weide, D. W., "Frequency-comb infrared spectrometer for rapid, remote chemical sensing," *Optics Express* **13**, 9029–9038 (Oct 2005).

[2] Keilmann, F. and Amarie, S., "Mid-infrared frequency comb spectroscopy," *Nature Photonics* **6**, 174–181 (2012).

[3] Kippenberg, T. J., Gaeta, A. L., Lipson, M., and Gorodetsky, M. L., "Dissipative Kerr solitons in optical microresonators," *Science* **361**(6402) (2018).

[4] Coen, S., Randle, H. G., Sylvestre, T., and Erkintalo, M., "Modeling of octave-spanning Kerr frequency combs using a generalized mean-field Lugiato–Lefever model," *Physical Review A* **87**(5), 053852 (2013).

[5] Chembo, Y. K. and Menyuk, C. R., "Spatiotemporal Lugiato–Lefever formalism for Kerr-comb generation in whispering-gallery-mode resonators," *Physical Review A* **87**, 053852 (May 2013).

[6] Simsek, E., Niang, A., Islam, R., Courtright, L., Shandilya, P., Carter, G. M., and Menyuk, C. R., "A mixed-field formulation for modeling dielectric ring resonators and its application in optical frequency comb generation," *Scientific Reports* **15**(1), 35098 (2025).

[7] Simsek, E., Niang, A., Shandilya, R. P., Islam, R., Courtright, L., Carter, G. M., and Menyuk, C. R., "One-stop-shop for modeling optical frequency comb generation," in [*Proceedings of the 26th International Conference on Electromagnetics in Advanced Applications (ICEAA)*], (Sep 2025).

[8] Edwards, D. F. and Ochoa, E., "Infrared refractive indexes of silicon," *Applied Optics* **19**(24), 4130–4131 (1980).

[9] Querry, M. R., "Optical constants of minerals and other materials from the millimeter to the ultraviolet," Tech. Rep. CRDEC-CR-88009, U.S. Army Armament Research and Development Command, Chemical Research, Development and Engineering Center, Aberdeen (1987).

[10] Simsek, E., "Practical vectorial mode solver for dielectric waveguides based on finite differences," *Optics Letters* **50**, 4102–4105 (Jun 2025).

[11] Simsek, E., "Finite-differences-based solvers for wave propagation in dielectric waveguides and rings," in [*2025 International Applied Computational Electromagnetics Society Symposium (ACES)*], 1–2 (2025).